Journal of Alloys and Compounds 885 (2021) 161109

Contents lists available at ScienceDirect

Journal of Alloys and Compounds

journal homepage: www.elsevier.com/locate/jalcom

Corrosion and tribocorrosion behaviour of Ti-B_4C composites processed by conventional sintering and hot-pressing technique

L. Sousa[a,b,*], A.C. Alves[a,c], A. Guedes[a,d], F. Toptan[a,c,e,*]

[a] CMEMS-UMinho – Center of MicroElectroMechanical Systems – Universidade Minho, Campus de Azurém, Guimarães, Portugal
[b] DEMM – Department of Metallurgical and Materials Engineering – Faculdade de Engenharia da Universidade do Porto, Porto, Portugal
[c] IBTN/Euro – European Branch of the Institute of Biomaterials, Tribocorrosion and Nanomedicine, Dept. Eng. Mecânica, Universidade do Minho, Azurém, 4800–058 Guimarães, Portugal
[d] DEM-UMinho – Department of Mechanical Engineering – University of Minho, Campus de Azurém, Guimarães, Portugal
[e] Department of Materials Science and Engineering, Izmir Institute of Technology, Urla, Izmir 35430, Turkey

ARTICLE INFO

Article history:
Received 20 April 2021
Received in revised form 22 June 2021
Accepted 8 July 2021
Available online 10 July 2021

Keywords:
Titanium
Metal-matrix composites (MMCs)
Corrosion
Tribocorrosion

ABSTRACT

In this work, low volume reinforcement ex-situ Ti-B_4C composites were produced using two different routes: conventional powder metallurgy (PM) and hot-pressing (HP). The effect of reinforcement phases and processing method on corrosion and tribocorrosion behaviour were studied. Composites processed by PM lost the typical passive behaviour of Ti matrix, while composites processed by HP presented similar behaviour to unreinforced Ti. Tribocorrosion tests showed that both composite groups presented two times decrease in corrosion kinetics under sliding compared to pure titanium. An antagonistic effect between wear and corrosion was observed for composites with at least two times decrease in wear volume compared to titanium.

1. Introduction

Titanium (Ti) and its alloys are still among the most used materials in the fabrication of hip implants owing to their good corrosion resistance, biocompatibility and satisfactory mechanical strength [1,2]. However, the high susceptibility to the combined action of wear and corrosion (tribocorrosion) under the physiological environment is still a major concern. The release of Ti wear products together with the release of metallic ions to the surrounding tissue and blood can lead to a vast number of adverse effects including inflammations, cytotoxicity, genotoxicity, carcinogenicity, among other issues, all of which can lead to implant failure [3].

In the last years, titanium matrix composites (TMCs) intended for orthopaedic implants have started to receive attention. By introducing hard ceramic phases into a Ti matrix, it is possible to improve the wear resistance due to a combination of several factors such as the load carrying effect given by the reinforcement phases and by modifications in the microstructure of the matrix yielding with grain refinement, induced dislocations and Orowan strengthening mechanisms [4]. By introduction of such reinforcements, there is a general increase in Young´s modulus [5,6], which is the one of the main concern for load bearing biomedical implants. In addition, high volume of reinforcement phases, may also lead to other problems such as porosity, which not only degrade the mechanical properties but also may jeopardize the corrosion behaviour due to localized corrosion [7].

Boron carbide (B_4C) is among the most used reactants to produce in-situ TMCs, since the Ti+B_4C reaction leads to the formation of TiC and TiB and/or TiB_2 reinforcement phases. Thus it has been considered as excellent reinforcement for TMCs, mainly due to their compatibility and strong interfacial bonding with titanium together with similar coefficients of thermal expansion (CTEs), being 8.2×10^{-6}/°C for Ti, 7.2×10^{-6}/°C for TiB, and 7.9×10^{-6}/°C for TiC [8–10]. Due to its intrinsic properties such as high hardness, wear resistance, high thermal as well as high chemical stability, B_4C can also be used directly as a reinforcement, which has been widely used in the fabrication of Al-B_4C composites [11–14].

In a study by some of the present authors [15], Ti-24%vol. B_4C composites processed by hot-pressing showed promising results regarding tribocorrosion behaviour. Ti-B_4C composite not only showed significantly reduced wear volume loss compared to unreinforced Ti, but also presented lower susceptibility to corrosion as

* Corresponding authors at: CMEMS-UMinho – Center of MicroElectroMechanical Systems – Universidade Minho, Campus de Azurém, Guimarães, Portugal.
E-mail addresses: a65256@alunos.uminho.pt (L. Sousa), fatihtoptan@iyte.edu.tr (F. Toptan).

https://doi.org/10.1016/j.jallcom.2021.161109
0925-8388/

well as lower corrosion rates under sliding. However, due to high volume of reinforcement, bridging of reinforcement phases during processing lead to some porosity which than lead to discontinuities in the passive oxide film and a consequent reduction on the corrosion behaviour under static conditions.

Several processing techniques are used to process metal matrix composites (MMCs), which can be mostly divided in two distinct methods as solid- and liquid-phase processing routes. Solid-phase techniques offer several advantages compared to liquid-phase ones as lower processing temperatures, minimizing the undesirable chemical reactions, better matrix/reinforcement interfaces and excellent control over microstructure. Solid-state routes include techniques such as diffusion bonding, hot-rolling, extrusion and powder metallurgy (PM) [16,17].

PM based routes are attractive for the fabrication of both whisker and particle-reinforced MMCs, mainly due to its simplicity when compared to other manufacturing processes as well as the possibility to produce intricate shapes with high accuracy [17,18]. Press-and-sintering approach or pressureless sintering can be considered as the simplest and cost-effective conventional PM technique. Conventional PM processing route is divided in three main steps, namely, blending and mixing the powders, cold compaction and sintering [19]. However, these methods may have limited success due to poor densification of the resulting composites. In order to obtain composites with higher densification, more advanced techniques, such as HP and spark plasma sintering, can be used. In these methods, pressure and temperature are applied simultaneously, allowing better densifications, but also reduced processing times, thus finer grained microstructures and consequently better mechanical properties, although these techniques are associated with higher costs [17].

In recent years, extensive research has been made on additive manufacturing (AM) routes, which are based on 3D printing layer-upon-layer of the chosen material. The main advantage of AM techniques resides in the fact that they can produce complex and near net shape components with minimal material loss and minimal post processing. When it comes to fabrication of TMCs, AM techniques still face some challenges, such as the high melting point of Ti, which complicates processing, poor densification of composites with high volume of reinforcement and limitation on the size of reinforcement particles [20].

From conventional to the recent processing methods, the role of the processing route on the tribocorrosion behaviour of TMCs should be clearly understood before selecting the processing route for load-bearing biomedical implants. In this context, the main objective of this work was to do a comparative study between two different conventional powder technology techniques (pressureless sintering and hot-pressing) on the synergism between wear and tribocorrosion for low volume reinforcement Ti-B_4C composites.

2. Experimental

2.1. Materials and methods

Ti composites reinforced with 3% volume of B_4C particles were produced by two distinct routes by mixing c.p. titanium (grade 2) and B_4C powders, both with irregular shapes and average particle sizes of 25 and 30 µm. Particle size distributions were obtained by laser particle analyzer (Malvern Series 2600 and Mastersizer 2000) and the results are shown in Fig. 1. For samples produced by conventional PM (ø 12 mm, 3 mm thickness), the powders and 0.4 vol% of binder (PVA from Sigma Aldrich, Mowiol 8–88), were mixed in a ball mill containing Al_2O_3 balls (ø 10 mm) and operating at 120 rpm for 4 h under Ar atmosphere. The mixture was then cold compacted with a uniaxial pressure of 350 MPa during 2 min in a steel die (previously lubricated with zinc stearate). The green compacts were

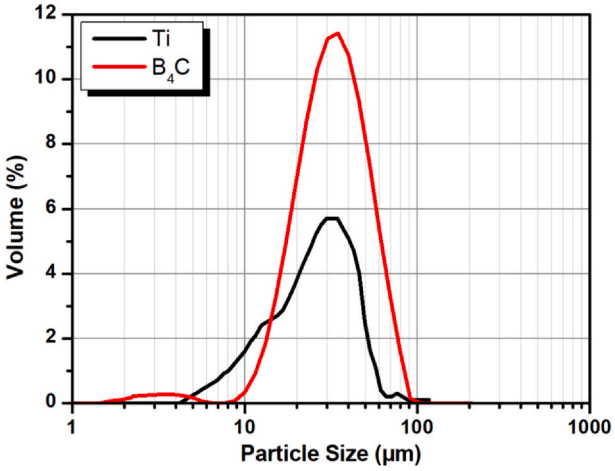

Fig. 1. Particle size distribution for Ti and B_4C powders.

placed in a tubular furnace under Ar atmosphere and heated to 450 °C, at a rate of 5 °C.min^{-1}, for the binder elimination. After a 3 h stage at this temperature the green compacts were cooled down to room temperate at 5 °C.min^{-1}. Samples were then pressureless-sintered at 1100 °C for 3 h under high vacuum atmosphere (< 10^{-5} mbar) with heating and cooling rates set at 5 °C.min^{-1}.

HP samples (ø 10 mm, 3 mm thickness) were produced by mixing the powders under the same conditions without the addition of binder. After mixing, the powder blends were poured into a graphite die. In order to avoid chemical reactions between Ti and graphite, the die walls were previously coated with zirconia paste. HP was then performed under high vacuum atmosphere (< 10^{-5} mbar) and under an applied pressure of 40 MPa. The sintering stage was performed at 1100 °C for 30 min, with heating and cooling rates set to 5 °C.min^{-1}and 10 °C.min^{-1}respectively. For both processing techniques, Ti samples were also produced and were used as control groups.

Prior to each test, samples were grinded down to 2400 mesh with SiC papers and then polished down to 0,04 µm with colloidal silica suspension (Struers). Afterwards, samples were cleaned in an ultrasonic bath with propanol and distilled water for 10 and 5 min, respectively, and finally dried with warm air. Before each corrosion and tribocorrosion test, the samples were kept in a desiccator for a period of 24 h to assure similar surface conditions. In this paper, samples processed by conventionally powder metallurgy are designated as Ti_PM and Ti-3B_4C_PM, whereas samples processed by hot-pressing are designated as Ti_HP and Ti-3B_4C_HP.

2.2. Electrochemical tests

Electrochemical tests were performed in a conventional three electrodes electrochemical cell (adapted from ASTM: G3–89) containing 0.9 wt% NaCl solution at body temperature (37 ± 2 °C) as one of the main constituents of physiological solutions [21–23]. The samples were connected as working electrode (WE), with an exposed area of 0.38 cm^2, while a saturated calomel electrode (SCE) and a Pt wire were used as reference electrode (RE) and counter electrode, respectively. The electrochemical tests consisted in OCP measurements until stabilization (ΔE < 60 mV.h^{-1}), followed by EIS measurements performed at OCP and finally by potentiodynamic polarization tests. A Gamry Potentiostat/Galvanostat/ZRA (model Referece-600+) was used in all the tests. EIS data were obtained by scanning a frequency range starting from 10^5 until 10^{-2} Hz, with 10 points per frequency decade and an amplitude of the sinusoidal signal of 10 mV. Impedance data was fitted using Gamry Echem Analyst software (version 5.61) to the electrical equivalent circuits

(EEC) and its quality of fitting was evaluated trough the values of goodness of fitting. After EIS measurements, potentiodynamic polarization scans were performed in the anodic direction with a rate of 1 $mV.s^{-1}$, from − 0.9 up to 1 V_{SCE}.

2.3. Tribocorrosion tests

Tribocorrosion tests were performed in the same NaCl solution at body temperature, placed inside a tribo-electrochemical cell. The samples slid against an alumina ball (ø 10 mm- Ceratec) in a tribometer (CETR-UMT-2) with a reciprocating ball-on-plate setup. Tribocorrosion tests were then carried out under three different conditions, namely, at OCP and under two distinct applied potentials: + 0.5 V_{SCE} (anodic potential - AP) and − 0.75 V_{SCE} (cathodic potential - CP). These potentials were chosen based on the results from potentiodynamic polarization tests in order to study the synergism between wear and corrosion. In this way, applying a potential in the cathodic domain, only the mechanical response from the system is given, considering the lubricant effect of the electrolyte. On the other hand, applying a potential in the passive region (anodic potential), response from mechanical wear and chemical wear can be accessed.

In order to access the susceptibility to corrosion under sliding, OCP values were measured before, during and after sliding using a two-electrode setup (SCE as RE and samples as WE). For potentiostatic tribocorrosion tests, current evolution was followed before, during and after sliding using three-electrodes setup as previously described. All electrochemical measurements were performed in a Gamry Potentiostat/Galvanostat/ZRA (model Referece-600). All tribocorrosion tests were performed under 1 N normal load (corresponding to a maximum Hertzian contact pressure of 0.41 GPa for c.p. Ti) during 30 min, with a stroke length of 3 mm and 1 Hz of frequency where coefficient of friction (COF) values during sliding were also followed. Before characterization, the worn surfaces were cleaned using the same procedure described previously.

2.4. Characterization

Microstructure was evaluated by field emission gun scanning electron microscope (FEI Nova 200), equipped with EDAX energy dispersive X-ray spectroscopy (EDS). Vickers macro-hardness tests were performed on an Officine Galileo Mod. D200 tester under 30 kgf of load during 15 s in order to calculate the overall hardness of the composites through 5 indentations made per sample (3 samples per condition). After tribocorrosion tests, the worn surfaces were characterized by using the same FEG-SEM/EDS and the wear track profiles were obtained by profilometry (Veeco, Dektak 150). The wear volume calculations followed the same procedure given elsewhere [24]. All the tests were at least triplicated to assure reproducibility and all the values are presented as average ± standard deviation. Phase analysis was determined by X-ray diffraction (XRD) on a Bruker AXS D8 Discover with Cu-Kα radiation (λ = 1,54060 Å), scanning from 15° to 80° at a speed of 0,04°/2 s. Once that the amount of reinforcement phases was under the XRD detection, Ti-24%vol. B_4C composites were processed by PM under identical conditions for structural analysis purposes. The porosity for composite groups was estimated by image analysis using ImageJ software (version 1.51j8) by considering a total area of 56 mm^2 for each group.

3. Results

3.1. Microstructure

The overall microstructure together with the EDS spectra obtained for both composites is shown in Fig. 2. The microstructure is composed of three distinct zones: black reinforcement particles (B_4C), light grey Ti matrix and dark grey reaction zone formed in between the B_4C particles and the Ti matrix. EDS spectra taken from these zones showed that the reinforcement particles were essentially composed of B and C; the Ti matrix consisted essentially of Ti and the reaction zone of Ti, B and C elements. Composites processed by PM presented much thicker reaction zones, and consequently smaller B_4C particles, compared to composites processed by HP, with some porosity between the reaction zone and the Ti matrix, while the same defects were hardly observed on the composites processed by HP. In fact, composites processed by PM presented much more porosity than composites processed by HP, i. e. 2.65 ± 0.80 for PM and 0.06 ± 0.02 % porosity for HP composites. Fig. 3 shows the XRD patterns obtained from Ti-24B_4C_PM where, besides Ti (ICDD 00-044-1294) and B_4C (ICDD 00-035-0798) peaks, peaks related to TiC (ICDD 00-031-1400) and TiB (ICDD 01-073-2148) phases were also detected. Table 1 shows the overall hardness for all groups. Comparing both Ti groups, Ti processed by PM presented significantly higher hardness than Ti processed by HP. Composites processed by PM presented similar hardness values to Ti processed by PM, while composites processed by HP presented higher hardness values compared to Ti processed by HP. Comparing composites groups, similar hardness values were observed.

3.2. Electrochemical behaviour

Representative potentiodynamic polarization curves for each group are presented in Fig. 4a and the average corrosion potential ($E_{(i=0)}$), open circuit potential (E_{OCP}) values (average values of the last 10 min of immersion) and passivation current density (i_{pass}), taken at 0.5 V are given in Table 2. Unreinforced Ti groups presented a well-defined passivation plateau due to the formation of the characteristic passive oxide film. On the other hand, while Ti-B_4C_HP presented very similar behaviour to unreinforced Ti with the passivation plateau starting at around 0.30 V, on Ti-B_4C_PM, a passivation region was observed, characterized by a slow increment on corrosion current density values. In addition, both groups processed by HP presented higher corrosion potential values (Table 2).

Bode and Nyquist diagrams are presented on Fig. 4b and c. On Bode diagrams, constant |Z| values and phase angles near 0° were observed in all groups for high frequency range (1–10 kHz), corresponding to the electrolyte resistance. For both unreinforced Ti and Ti-B_4C_HP groups, phase angles near − 90° were observed between low and middle frequency range indicating the formation of a compact passive oxide film. On the other hand, Ti-B_4C_PM composites presented phase angles near − 70°, indicating lower quality of the passive oxide film. The total impedance of the system is given by the values of $|Z|_{f\rightarrow 0}$, showing the corrosion resistance of the system. Unreinforced Ti groups and Ti-B_4C_HP composites presented very similar values (c.a. 4×10^5 $\Omega.cm^2$) while Ti-B_4C_PM composites showed values close to 10^4 $\Omega.cm^2$. On Nyquist diagrams, larger diameters correspond to higher overall corrosion resistance. When compared to unreinforced Ti groups, Ti-B_4C_HP composites presented slightly smaller diameter while Ti-B_4C_PM composites presented noticeably reduced corrosion resistance.

The EECs used to fit the EIS data are shown in Fig. 4d and Fig. 4e. For both unreinforced Ti groups and Ti-B_4C_HP, the EEC consists of an electrolyte resistance (R_e) and a pair (R_{ox}/Q_{ox}), corresponding to the resistance (R_{ox}) and CPE (constant phase element, Q_{ox}) of the native passive oxide film, respectively. For Ti-B_4C_PM composites, the EEC consists of an electrolyte resistance (R_e), the resistance and CPE of the oxide film (R_{ox} and Q_{ox}) and the processes taking place inside the pores. The later consisting of an additional electrolyte resistance ($R_e^{'}$), the charge transfer reaction due to localized corrosion (R_{ct}) and the capacitance of the double layer (Q_{dl}). R_{ox} was

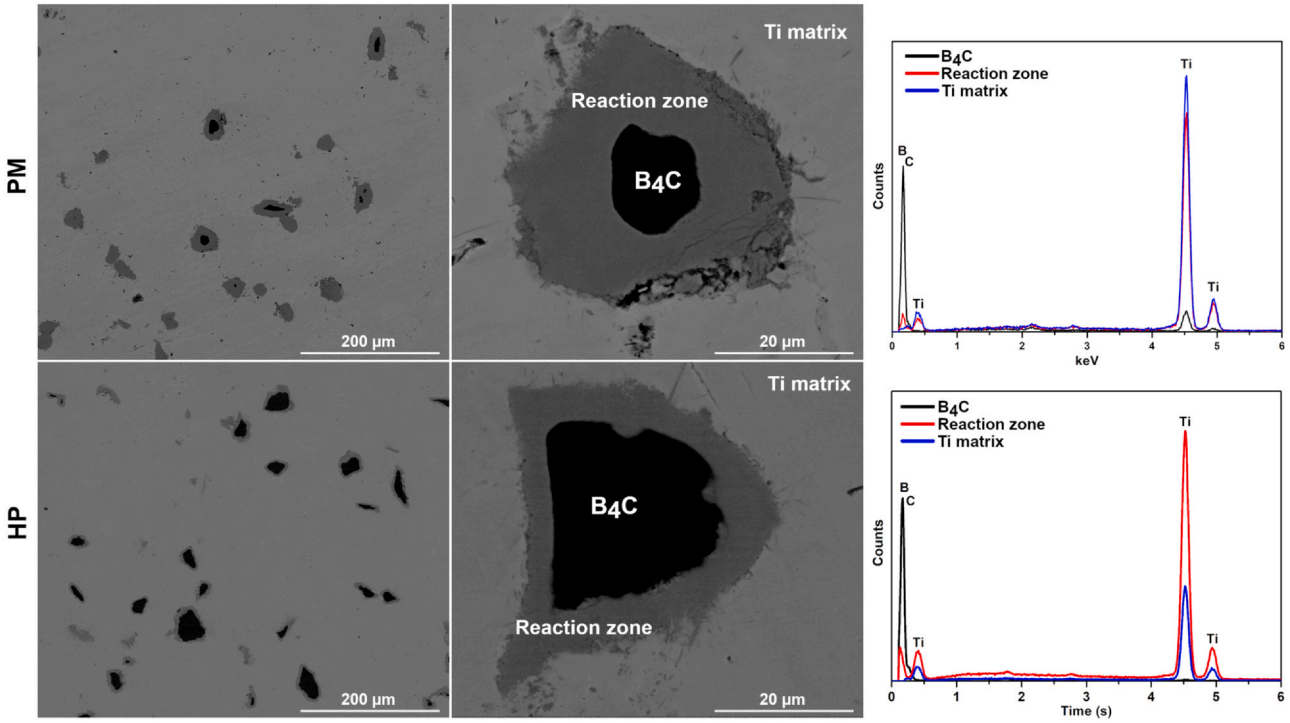

Fig. 2. Back-scattered electron (BSE) SEM images of the composites processed by PM and HP, together with EDS spectra taken from the B_4C particles, reaction zone and Ti matrix.

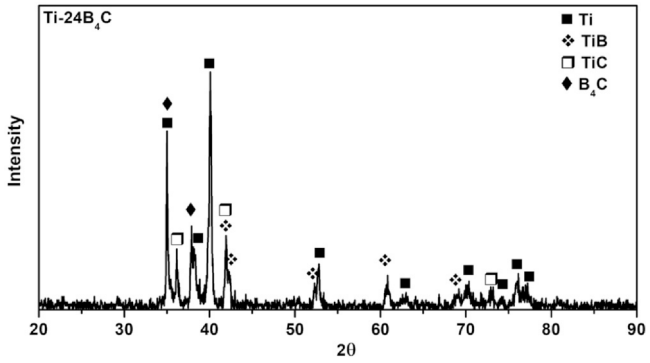

Fig. 3. XRD spectra obtained from a Ti-24%vol. B_4C composite processed under the same PM conditions.

Table 1
Hardness values obtained for both Ti and Ti-B_4C groups.

	Ti_PM	Ti_HP	Ti-3B_4C_PM	Ti-3B_4C_HP
HV_{30}	387 ± 18	285 ± 8	388 ± 25	401 ± 19

removed from the EEC due to its extremely high value and it does not allow the conduction of electrons inside the passive film.

In both EECs, a CPE was used to account for the deviation of an ideal capacitator, where the capacitance of the CPE is defined by $Z_{CPE} = [Y_0(jw)^n]^{-1}$, with $-1 \leq n \leq 1$ and $n = -1$ corresponding to an inductor, $n = 0$ to a resistor, $n = 1$ to a capacitator and, n values close to 1 representing a non-ideal capacitator. The quality of fitting was evaluated by their goodness of fitting values, where all values were below 10^{-4} indicating that the proposed EECs described adequately the behaviour of all the tested groups (fitting results are given on Table 3). Ti-B_4C_PM composites presented considerably higher Q_{ox} values compared to the other groups, indicating the lower quality of the oxide film. Comparing R_{ox} values, Ti-B_4C_HP composites presented lower values compared to unreinforced Ti groups, suggesting a relatively lower resistance of the passive layer formed on the composite surface.

3.3. Tribocorrosion behaviour

The evolution of OCP before, during and after sliding together with the respective evolution of coefficient of friction during sliding is given in Fig. 5a. All the groups presented stable OCP values before sliding due to a stable passive film. Immediately after sliding started, a sharp decrease in OCP values towards cathodic direction was observed for all the groups, as a result of the mechanical damage induced to the passive film and consequent formation of active zones leading to an increase in susceptibility to corrosion under the mechanical action. For unreinforced Ti groups, Ti_HP samples presented a sharp OCP drop of around − 0.73 ± 0.03 V, while Ti_PM presented an initial drop of − 0.38 ± 0.02 V and then a gradual decrease to values around − 0.65 ± 0.02 V.

Compared to unreinforced Ti groups, both composites presented lower OCP drops on the onset of sliding where Ti-B_4C_PM presented the lowest OCP drop of − 0.18 ± 0.05 V against the − 0.45 ± 0.03 V observed for Ti-B_4C_HP. During sliding, OCP values for Ti-B_4C_PM composites increased up to almost the starting potential during the first 600 s of sliding, remaining around the same values until the end of sliding. On the other hand, Ti-B_4C_HP composites presented significant fluctuations on OCP during sliding. Nonetheless, OCP values were still nobler than both unreinforced Ti groups. Immediately after sliding stopped, all the groups except Ti-3B_4C_PM, which already presented OCP values close to the starting ones, presented a gradual increase in OCP, reaching values close to the ones recorded before sliding started, due to repassivation of the worn area.

Regarding COF values, distinct behaviours were observed between samples processed by PM and HP. Unreinforced Ti_PM oscillated around similar values until the 500–600 s of sliding (around 0.45 ± 0.01), after that, COF values increased to around 0.71 ± 0.01, remaining close to this value until the end of sliding. For unreinforced Ti_HP, COF values also started at around 0.39 ± 0.01, however, after a few seconds (between 10 and 100 s), COF values

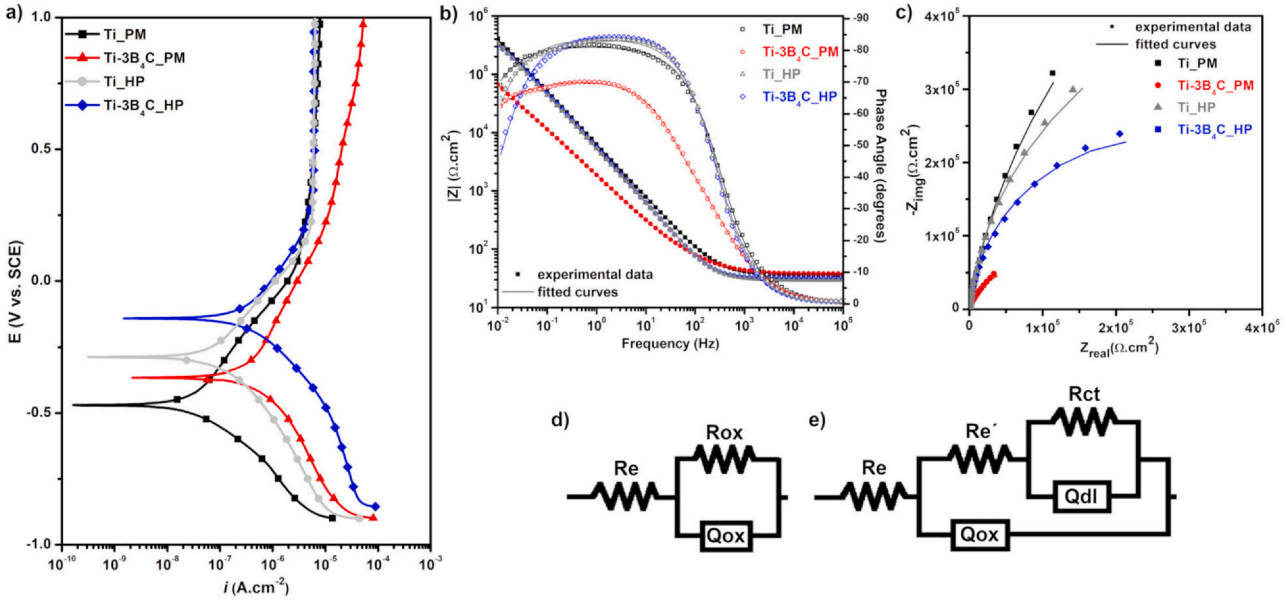

Fig. 4. Corrosion results: a) Representative potentiodynamic polarization curves, b) Bode diagrams, c) Nyquist diagrams, and EECs used for d) Ti_PM, Ti_HP and Ti-3B_4C_HP groups and for e) Ti-3B_4C_PM group.

Table 2
Corrosion potential ($E_{(i=0)}$), open circuit potential (E_{OCP}) and passivation current density (i_{pass}) values.

	Ti_PM	Ti_HP	Ti-B_4C_PM	Ti-B_4C_HP
i_{pass} (μA cm^{-2})	5.34 ± 0.70	5.86 ± 0.17	34.63 ± 5.40	6.05 ± 0.17
E_{OCP} (V)	−0.36 ± 0.01	−0.24 ± 0.01	−0.15 ± 0.07	−0.19 ± 0.03
$E_{(i=0)}$ (V)	−0.44 ± 0.04	−0.28 ± 0.01	−0.25 ± 0.02	−0.14 ± 0.02

increased to around 0.58 ± 0.02 and oscillated around these values during almost the entire period of sliding, although a few drops were observed. Ti-B_4C_PM composites presented a run-in period of around 200 s, where COF values increased from 0.34 ± 0.02–0.59 ± 0.02. After that, COF values slowly increased to around 0.70 and remained around these values until the end of sliding. Ti-B_4C_HP composites did not show any distinct run-in period, instead, a gradual increase in COF values was observed during the first 1500 s, after that COF values stayed at around 0.52 ± 0.05.

Fig. 5b shows the representative evolution of anodic current at a constant applied potential before, during and after sliding together with the respective evolution of COF. Before sliding, all the groups presented stable current density values due to presence of a stable passive oxide film. While Ti_PM, Ti_HP and Ti-3B_4C_HP groups presented similar current density values before sliding started, Ti-3B_4C_PM group presented higher values, which is in accordance to what was observed on the potentiodynamic polarization curves. Between all the conditions, unreinforced Ti groups presented higher increase in current density values on the onset of sliding where Ti_HP samples showed the highest increase. On the other hand, both composite groups increased to similar current density values c.a. 0.30 μA.cm^2. The anodic charge, Q, was calculated by integrating the current density values obtained during sliding, using the average current density before sliding as baseline, and the values were found as (5.65 ± 0.92) x 10^{-5}, (6.81 ± 1.33) x 10^{-5}, (3.02 ± 0.53) x 10^{-5}, and (3.67 ± 0.37) x 10^{-5} C/cm^2 for Ti_PM, Ti_HP, Ti-3B_4C_PM and Ti-3B_4C_HP respectively. Composite groups presented very similar values independently of processing method, while Ti_PM presented slightly lower Q values compared to Ti_HP. Overall, composites presented approximately 2 times decrease in Q values suggesting decreased corrosion kinetics under sliding coming from the wear track.

As it can be seen, under these conditions, all the groups presented a run-in period where COF values increased in the approximately first 200 s of sliding. During roughly the same period, all the groups also showed a significant decrease in current density values. Overall, Ti-B_4C_PM presented the highest corrosion current density values during sliding. Despite the higher increase in current density values that were observed for both Ti samples after sliding started, after some time, current density values dropped down to values close to the ones registered before sliding, remaining relatively stable until the end of sliding. Ti-3B_4C_HP composites presented current density values between both unreinforced Ti groups and Ti-3B_4C_PM composites.

Representative secondary and backscattered electron SE/BSE SEM images of the worn surfaces, together with SE/SEM images and EDS spectra of the counter-body for all the groups after tribocorrosion tests performed under OCP can be seen on Fig. 6. For both unreinforced Ti groups tested under OCP, wear tracks presented ploughing grooves parallel to the sliding direction, which are an indication of an abrasive action of the transferred material to the counter-body due to adhesive wear. Discontinuous tribolayers were also observed within the wear tracks due to continuous oxidation and compaction of material being transferred between the two

Table 3
EEC parameters obtained from EIS data.

	Q_{ox} (x 10^{-5} s^n $\Omega^{-1}cm^{-2}$)	n_{ox}	Q_{dl} (× 10^{-6} s^n $\Omega^{-1}cm^{-2}$)	n_{dl}	R_{ox} (×10^6Ωcm^2)	R_{ct} (× 10^6Ωcm^2)
Ti_PM	16.32 ± 1.00	0.90 ± 0.01	-	-	1.47 ± 0.74	-
Ti_HP	21.99 ± 1.07	0.93 ± 0.01	-	-	0.76 ± 0.18	-
Ti-3B_4C_PM	38.65 ± 11.99	0.76 ± 0.04	12.61 ± 0.97	0.92 ± 0.06	–	0.73 ± 0.37
Ti-3B_4C_HP	20.84 ± 1.33	0.94 ± 0.01	-	-	0.47 ± 0.03	-

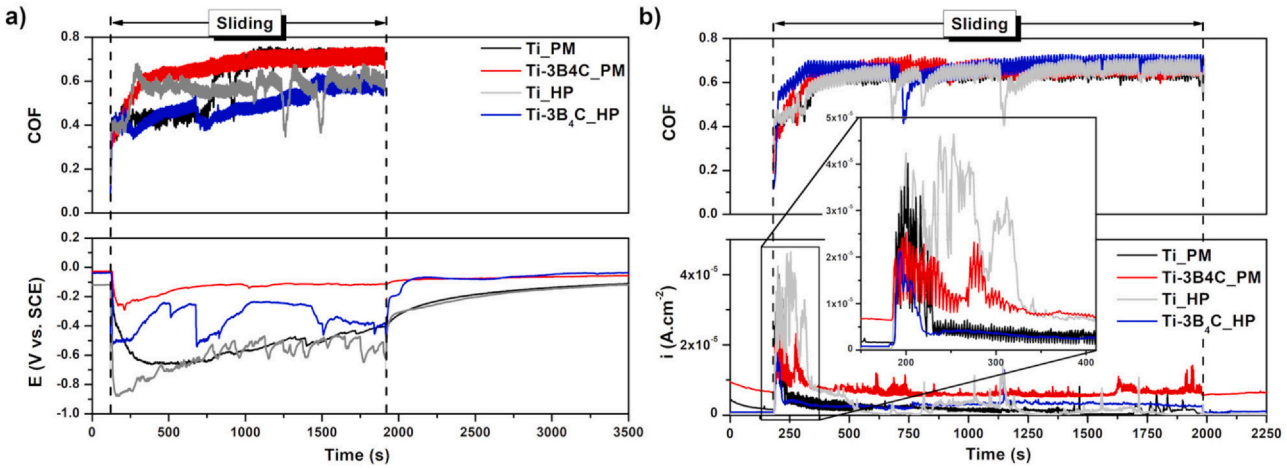

Fig. 5. Evolution of a) OCP and b) anodic current density before, during and after sliding together with the corresponding evolution of COF during sliding.

mating surfaces. In addition, scratch marks due to abrasion action of loose wear debris within the wear track were also observed for both Ti groups. Both composites presented similar features, with SE/SEM images suggesting less wear damage and no evidence of reinforcement particle pull-out was observed under these conditions. EDS spectra taken from the counter-body surfaces confirmed the transference of Ti between the two mating surfaces for all the tested groups, thus confirming the presence of adhesive wear. However, wear scars were relatively larger for unreinforced Ti samples, suggesting increased wear compared to composites.

Similar to what was observed for tribocorrosion tests performed under OCP, under the anodic domain, Fig. 7, all the groups also presented discontinuous tribolayers within the wear track. Ploughing grooves, on the other hand, were less pronounced for these conditions. In addition, the visible wear damage on the composite surfaces were significantly less on the low magnification SE images. EDS spectra from the counter-body also confirmed the presence of adhesive wear, however, the wear scars for all the groups were also considerably smaller than the ones observed under OCP, suggesting reduced wear. For tribocorrosion tests performed on the cathodic domain, Fig. 8, ploughing wear grooves were the more prevalent wear feature and discontinuous tribolayers were still present, hence, EDS spectra revealed that material transfer (adhesion) between the two sliding surfaces also occurred.

Representative 2D profiles taken from the worn surfaces and wear volume values are presented in Fig. 9. All the tested groups presented the same trend in wear volume loss under the different applied potentials, where higher wear volume losses were obtained under the cathodic domain, whereas the lowest values were obtained under the anodic domain. For all the conditions, composites presented lower wear volume losses compared to unreinforced Ti. Regarding processing methods, no clear trend was observed. Composite groups presented similar wear volume loss values under the different applied potentials. Comparing both Ti groups, particular differences were observed for the tribocorrosion tests performed under the cathodic domain, where Ti_HP presented considerably higher wear volume loss.

4. Discussion

The reaction between Ti and B_4C powders in both composites produced by PM and HP routes revealed a reaction zone around the B_4C reinforcements particles, containing Ti, B and C elements. XRD analysis on Ti-24B_4C_PM composites revealed the formation of TiB and TiC phases. The formation of TiB and TiC phases on Ti-24%vol B_4C composites by HP was also reported previously by some of the present authors [15]. The Ti-B_4C system is characterized by the formation of TiB_2, TiB and TiC phases, which belong to the Ti-B-C system [25,26]. Due to its lower Gibbs free energy (ΔG) and enthalpy (ΔH), TiB_2 is more likely to be formed in preference of TiB, however, due to limited mass transport rate in solid-state sintering, the main products of Ti-B_4C reaction are almost always TiC and TiB [26]. In this way, in addition to the mechanical entrapment of the B_4C reinforcement particles into the Ti matrix, a chemical bond was also formed. The reaction zones formed on the PM composites were much thicker than the ones observed on the HP composites, that may be explained by the increased sintering time (3 h for PM vs 30 min for HP) and consequently more time for the reaction between Ti and B_4C to take place. Once B_4C is consumed in the reaction, B_4C reinforcement particles tended to be smaller on the PM composites.

In MMCs, interfacial reactions between the matrix and reinforcement phases play an crucial role on the final mechanical properties of the composite and may have a beneficial or detrimental effect [27,28]. Currently, the main motivation of the Ti-B_4C system is to use B_4C as a reactant to produce in-situ TMCs, where the reaction products of the Ti + B_4C system (TiB, TiC and TiB_2) act as reinforcement phases [8–10,29,30]. In this way, the role of these reaction zones on the mechanical properties of ex-situ Ti-B_4C composites is still not completely understood. Nonetheless, the mechanical properties of TMCs reinforced with either TiB or TiC or even both phases is widely reported. Both TiB whiskers and TiC particles are reported to improve several mechanical properties, such as yield strength [31,32], ultimate compressive strength [32,33], tensile strength, creep resistance [8,34–36]. Furthermore synergistic effects between TiB and TiC have also been reported, meaning that TMCs reinforced by both TiB and TiC exhibit better mechanical behaviour over sole TiB or sole TiC reinforced TMCs [5].

Hardness values obtained for Ti_PM were considerably higher than the ones observed for Ti_HP. Ti and Ti alloys processed by different processing routes can present different hardness values [37]. Due to high affinity of Ti with oxygen, interstitial oxygen contamination is present in almost every step of processing, including mixing and debinding [38]. In this way, the increased hardness obtained on PM samples may be explained by the additional processing steps involved, including pressing and handling of the green compact, the use of binder and the debinding cycle.

By introducing the reinforcement particles, it would be expected that composites would present significantly higher hardness than their Ti counterparts, however this was not the case for composites processed by PM, where composites presented similar hardness values to unreinforced Ti. During the sintering stage, ceramic particles may hinder the sintering process and consequently reduce the

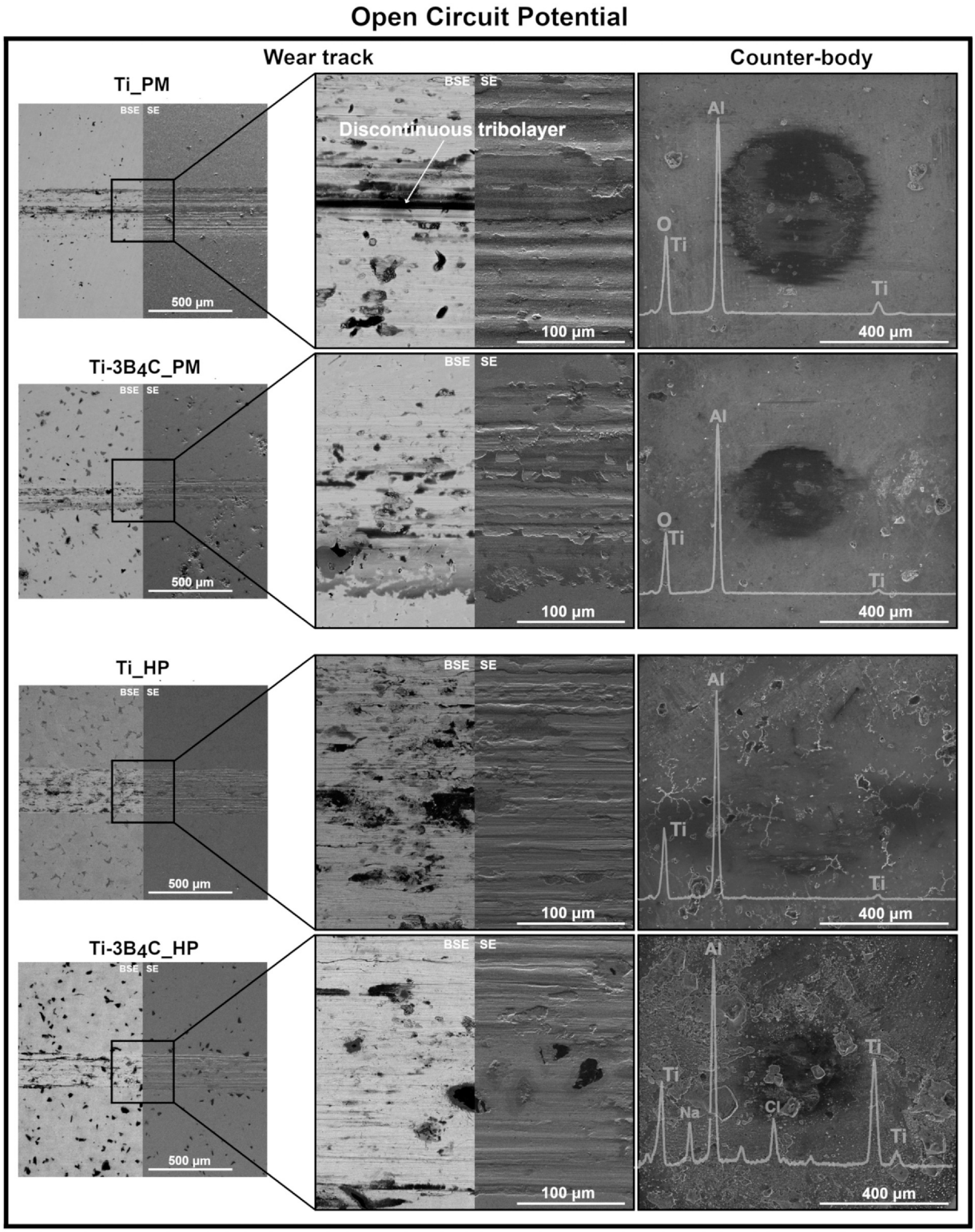

Fig. 6. SE/BSE SEM images of the wear tracks and respective counter-bodies for tribocorrosion tests performed under OCP.

densification of the composite, leading to higher amount of residual porosity [39]. Furthermore, it has also been reported that the volume reduction from the conversion of B_4C to TiB and TiC phases [40] may also lead to porosity and thus lower overall hardness values. In this way, the hardness values obtained for Ti-3B_4C_PM group is most probably related with the antagonistic effect between the introduction of reinforcement particles and porosity observed in these composites. The drawback of pressureless sintering approach was clearly observed in this work since composites presented similar hardness values to Ti due to considerable amount of porosity. Higher porosity for TMCs processed by pressureless sintering was also reported by Patel et al. [41] where the authors compared the microstructure of Ti-TiB_2 composites processed by pressureless and pressure assisted PM routes and reported increased porosity for the pressureless route. The authors also reported that by increasing sintering temperature porosity could be reduced. Due to applied

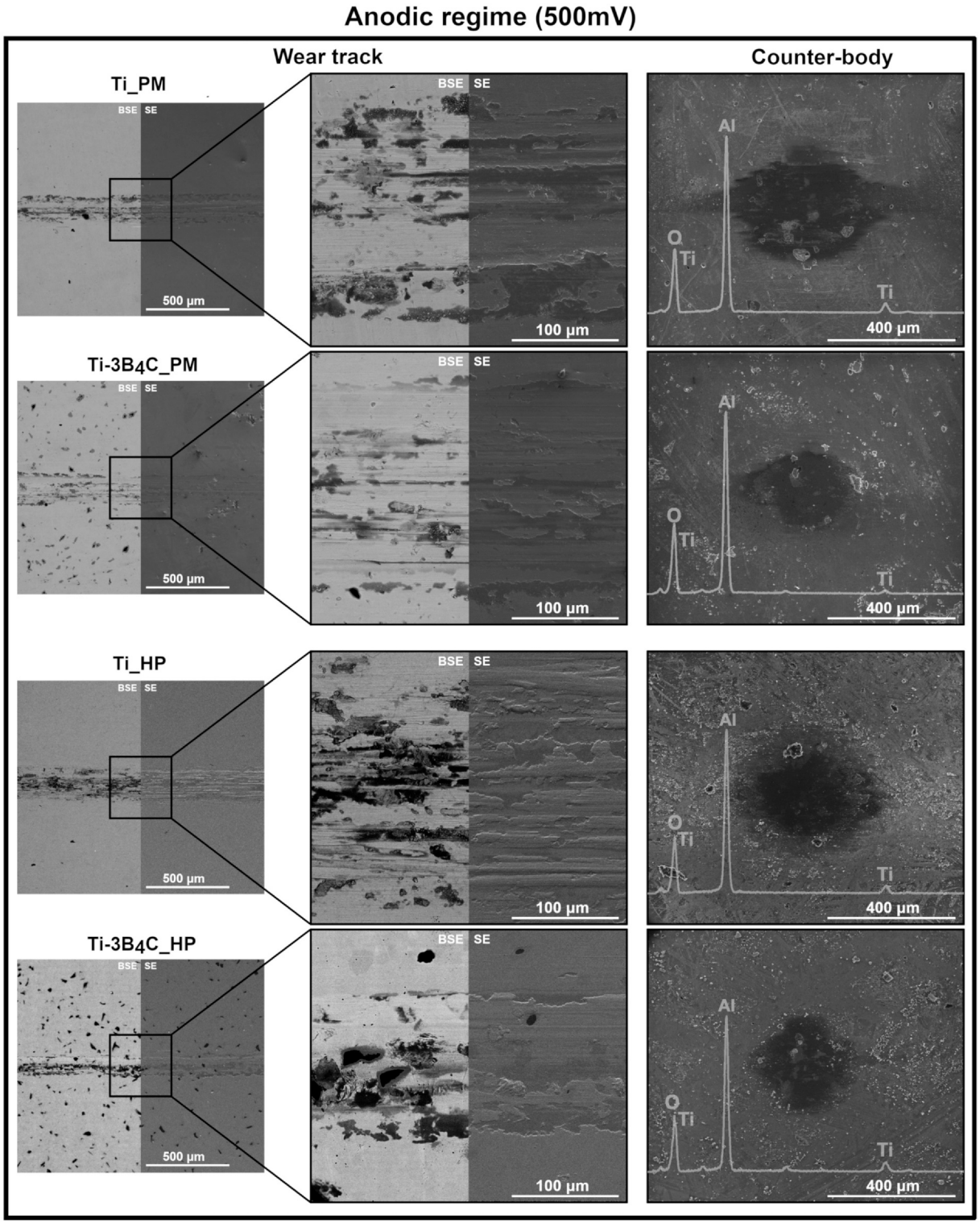

Fig. 7. SE/BSE SEM images of the wear tracks and respective counter-bodies for tribocorrosion tests performed under 500 mV (anodic regime).

pressure on HP technique, the negative effect of porosity was reduced and consequently composites showed a significant increase in hardness compared to Ti.

In MMCs, galvanic coupling between matrix and reinforcement or interfacial reaction layer may lead to a significant decrease on corrosion resistance. In addition to gaps at the matrix/reinforcement interface, microstructural defects may also have a substantial impact on the corrosion resistance of the base material, due to formation of discontinuities or heterogeneities on the protective passive film [42,43]. However, literature shows that MMCs may also present increased corrosion resistance since reinforcement phases may act as inert physical barriers against corrosion [44]. Additionally, it has also been reported that the introduction of reinforcement phases cause grain refinement leading to higher stability of the passive film [45].

In this work, it was possible to observe that Ti-B_4C composites processed by different routes had distinct behaviours. Composites

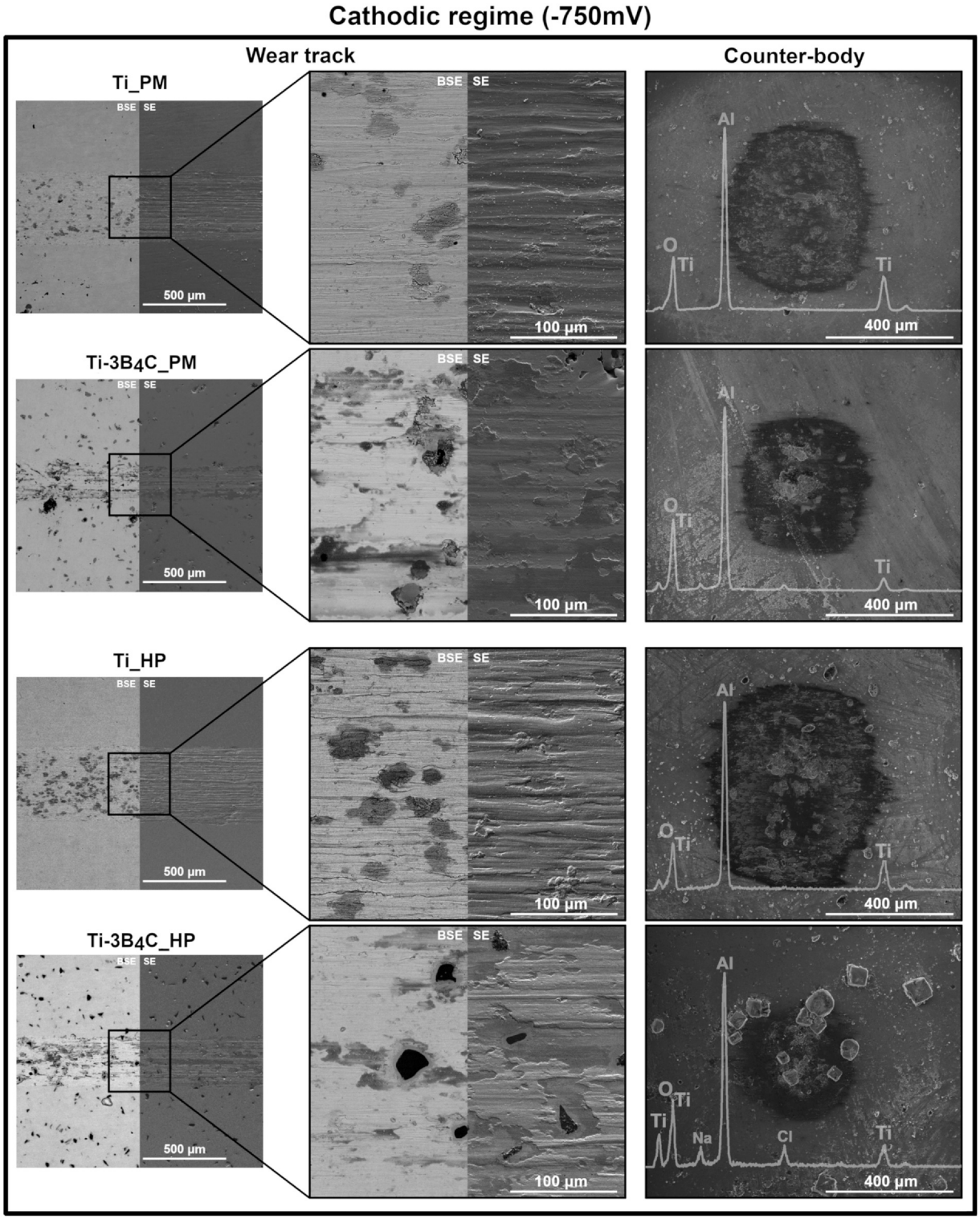

Fig. 8. SE/BSE SEM images of the wear tracks and respective counter-bodies for tribocorrosion tests performed under − 750 mV (cathodic regime).

processed by HP presented very similar corrosion behaviour to that of Ti, while composites processed by pressureless sintering showed notably reduced corrosion resistance, not only compared to the same composite processed by HP but also to Ti processed by the same route. Consequently, an alternative EEC had to be used to fit EIS data. Regarding the reaction products that were obtained for both composites (TiB and TiC), some studies reported that these phases do not have a negative effect on the corrosion resistance of Ti. In a study by Silva et al. [46], it was reported that the corrosion behaviour of in-situ Ti-TiB-TiN_x composites processed by HP was slightly better than unreinforced Ti due to the barrier role given by the reinforcement phases. Chen et al. [45] reported that Ti-TiB composites processed by selective laser melting (SLM) presented improved corrosion behaviour compared to Ti processed by the same method. The authors attributed the improved corrosion behaviour to the fact that TiB reinforcements acted as a micro-cathode during corrosion, which facilitated and accelerated the formation of the passive oxide film on the surface of the composites. Regarding TiC, some studies showed

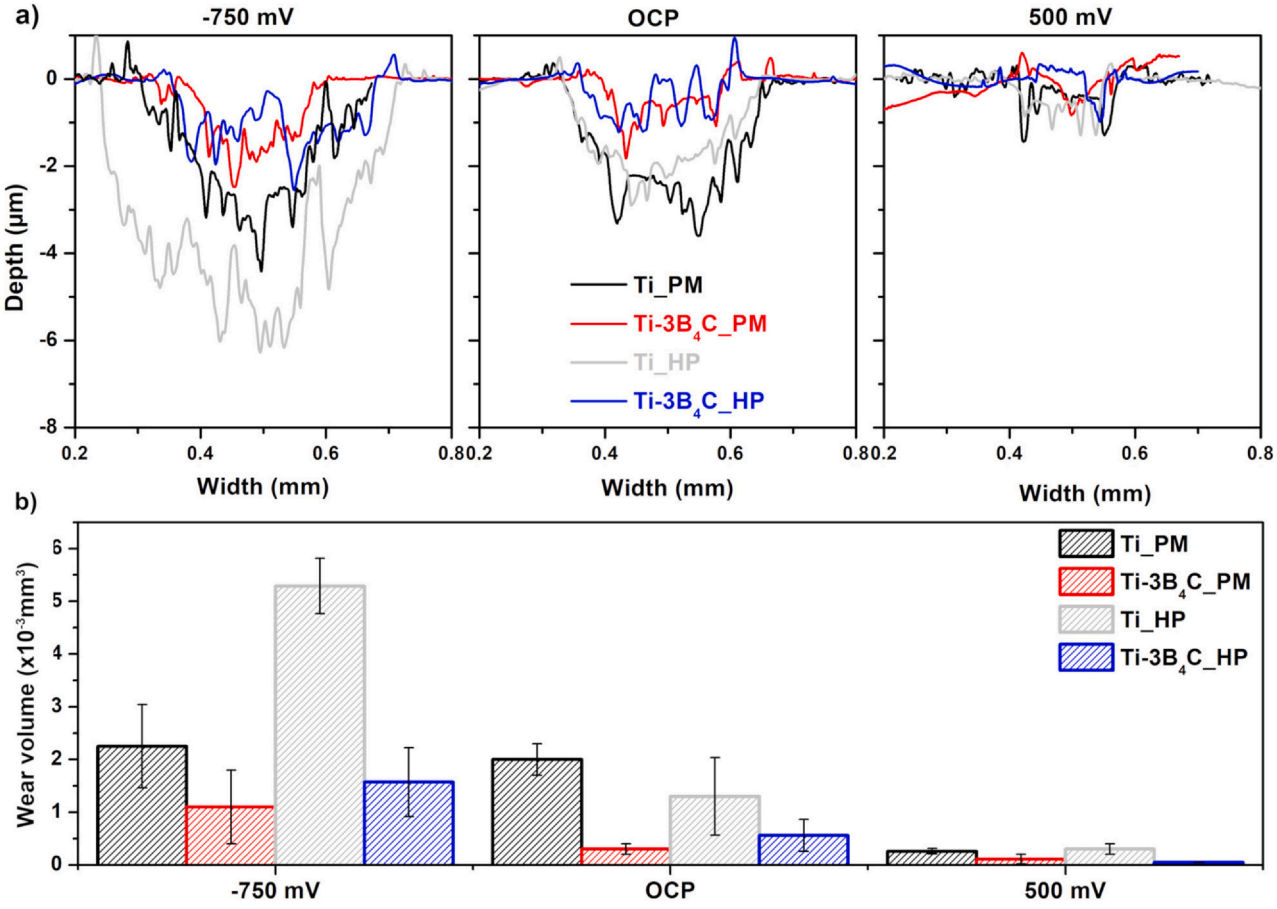

Fig. 9. a) Representative wear profiles for all the testes groups and tribocorrosion conditions together with b) average wear volume loss values calculated from wear profiles.

that Ti-TiC composites have very similar corrosion behaviour to unreinforced Ti [47,48].

In a previous study by some of the present authors [49], the electrochemical behaviour of Ti-24%vol. B_4C composites processed by hot-pressing was evaluated. It was reported that composites presented slightly reduced corrosion resistance compared to unreinforced Ti that was attributed to the porosity formed due to bridging of the agglomerated reinforcement particles, that consequently induced localized corrosion. In addition, interfacial gaps at the matrix/reinforcement interface, as well as pore sites, may lead to discontinuities on the passive film and/or different states of the passive film. Processing parameters as well as amount of reinforcement phases may also significantly change the corrosion behaviour of composites since they may lead to different densification rates and microstructures.

In this study, it was clear that Ti-B_4C_PM presented lower corrosion resistance compared to other tested groups. Considering that the corrosion behaviour of Ti-3B_4C_HP composites was very close to that of Ti, it is reasonable to assume that the reduced corrosion behaviour observed on Ti-B_4C_PM composites may be due to a combination of different factors, being the porosity associated with PM processing technique and/or the increased thickness of the reaction layers, which may be the cause for the overall lower quality of native oxide film. In a previous study by some of the present authors [50], the corrosion behaviour of Ti-B_4C composite processed by pressureless sintering using identical processing conditions was also reported, where the authors tested the composites by cyclic polarization scan and observed reduced corrosion current density in the reverse scan indicated that no susceptibility to localized corrosion was present in the system. However, the increased corrosion kinetics was due to microstructural defects between the matrix and the reaction zone, which compromised the integrity of the passive oxide film. Nonetheless, in order to make a definitive conclusion, further studies by local electrochemical techniques are needed to link better the microstructure with the electrochemical response.

Tribocorrosion tests showed that the introduction of B_4C reinforcement particles had a significant effect on the tribocorrosion behaviour of Ti. Both composites showed a decrease in tendency to corrosion under sliding, which may be mainly attributed to the load carrying effect given by the reinforcement phases. The fluctuations in COF and OCP values can be attributed to the formation, thickening, and breaking of discontinuous tribolayers during sliding. The presence of tribolayers within the wear tracks can lead to increased roughness and consequently higher COF values during sliding. When these tribolayers eventually reach a critical point and break, exposing new fresh metallic area to the electrolyte, a consequent decrease in OCP and COF is observed [46,51–53]. As it could be observed in the OCP evolution, this phenomenon was more prevalent on Ti-3B_4C_HP composites, whereas OCP and COF values were more stable for Ti-3B_4C_PM composites.

The evolution of anodic current density under sliding showed that, despite the current density peaks observed on the onset of sliding, after a few minutes, current density values decreased and stabilized at almost the same current density values observed before sliding. Under the anodic applied potential, the formation of tribolayers was promoted since the growth of the native passive oxide film was accelerated. As a result, the overall COF values were higher, possibly due to increased formation of the discontinuous tribolayers and consequently increased roughness. In addition, COF values were also more stable during sliding, in other words, after a run-in period,

oscillated around similar values till the end of sliding since the growth and stability of these tribolayers was promoted under the anodic potentiostatic control. It is known that these tribolayers can either play a beneficial and/or detrimental role during tribocorrosion. Due to higher hardness of these layers, they may play a limited protective role owing to load bearing effect and consequently reducing electrochemical active zones within the wear track. On the other hand, if these oxides break and roll freely on the wear track, they may act as a third-body abrasives and increase the mechanical wear [37,39,49,54]. In tribocorrosion, the total wear volume loss due to wear and corrosion cannot be simply calculated by the sum of material lost due to wear and material lost due to corrosion, since synergetic or antagonist effect may occur. The effect of corrosion on wear and the effect of wear on corrosion should also be considered, as these can significantly change the total wear volume loss. In the synergetic approach the total wear volume loss due to tribocorrosion can be described as the sum between material lost due to wear, material lost due to corrosion and the material lost due to the interplay between wear and corrosion. In most cases, a synergetic effect is observed, meaning that wear increases material lost to corrosion and vice-versa [55]. Based on the tribo-electrochemical and wear volume loss results, it is reasonable to state that under the tested conditions, an antagonistic effect was observed since the oxide layers formed during sliding had a beneficial role on the tribocorrosion behaviour of both Ti and composite groups. All the tested groups presented considerably higher wear volume loss under the cathodic potentials. Under cathodic potentials, the corrosion processes are inhibited, thus, the native oxide film is not allowed to growth, limiting the formation of load carrying tribolayers during sliding.

In fact, comparing the wear volume loss values against the ones observed for tribocorrosion tests under OCP and the cathodic domain, considerably less wear volume loss was observed on the anodic domain. The considerable higher wear volume loss observed for Ti_HP compared with Ti_PM under the cathodic domain can be explained by the lower hardness values, since mechanical wear is the main response of the system under these conditions. Under OCP and anodic potential, such differences were not observed, suggesting that the formation of tribolayers played a considerable role in wear resistance. Overall, composites presented considerably lower wear volume losses in all the conditions compared to Ti, independently of processing method. Within the composite groups, wear volume values were in range of the standard deviation of each other, which is in accordance with the hardness values.

5. Conclusions

Within the scope of this study, it was possible to conclude that the introduction of low amount of B_4C reinforcement particles into a Ti matrix can improve the overall tribocorrosion behaviour of Ti through reduced wear volumes, reduced tendency to corrosion, as well as reduced corrosion kinetics under sliding. Based on the results, it was possible to see that independently of processing method, under these conditions, Ti and composites showed an antagonistic effect between corrosion and wear, evidenced by the lower wear volume values obtained under the anodic domain. Additionally, it was possible to see that the overall microstructure of these composites played an important role on the corrosion behaviour, that was evidenced by the considerably lower corrosion resistance of the composites processed by PM.

CRediT authorship contribution statement

L. Sousa: Methodology, Validation, Formal analysis, Investigation, Writing – original draft. **A.C. Alves:** Methodology, Validation, Writing – review & editing. **A. Guedes:** Conceptualization, Validation, Formal analysis, Visualization, Supervision. **F. Toptan:** Conceptualization, Methodology, Writing – review & editing, Supervision.

Declaration of Competing Interest

The authors declare that they have no known competing financial interests or personal relationships that could have appeared to influence the work reported in this paper.

Acknowledgements

This work was supported by Portuguese Fundation for Science and Techonology (FCT), Portugal, under UIDB/04436/2020 and M-ERA-NET/0001/2015 projects. L. Sousa was grateful for the PhD grant through NORTE-08-5369-FSE-000051 project. The authors would like to acknowledge Prof. José Carlos Teixeira (University of Minho) for the provision of laser diffraction equipment.

References

[1] X. Liu, P.K. Chu, C. Ding, Surface modification of titanium, titanium alloys, and related materials for biomedical applications, Mater. Sci. Eng. R. Rep. 47 (2004) 49–121.
[2] S.C. Tjong, Y.W. Mai, Processing-structure-property aspects of particulate- and whisker-reinforced titanium matrix composites, Compos. Sci. Technol. 68 (2008) 583–601.
[3] I. Swiatkowska, N. Martin, A.J. Hart, Blood titanium level as a biomarker of orthopaedic implant wear, J. Trace Elem. Med. Biol. 53 (2019) 120–128.
[4] F. Saba, F. Zhang, S. Liu, T. Liu, Reinforcement size dependence of mechanical properties and strengthening mechanisms in diamond reinforced titanium metal matrix composites, Compos. Part B 167 (2019) 7–19.
[5] D.R. Ni, L. Geng, J. Zhang, Z.Z. Zheng, Fabrication and tensile properties of in situ TiBw and TiCp hybrid-reinforced titanium matrix composites based on Ti-B4C-C, Mater. Sci. Eng. A 478 (2008) 291–296.
[6] S. Gorsse, Y. Le Petitcorps, S. Matar, F. Rebillat, Investigation of the Young ' s modulus of TiB needles in situ produced in titanium matrix composite, Mater. Sci. Eng. A 340 (2003) 80–87.
[7] H. Tanigawa, H. Asoh, T. Ohno, M. Kubota, S. Ono, Electrochemical corrosion and bioactivity of titanium – hydroxyapatite composites prepared by spark plasma sintering, Corros. Sci. 70 (2013) 212–220.
[8] V.S. Balaji, S. Kumaran, Densification and microstructural studies of titanium–boron carbide (B4C) powder mixture during spark plasma sintering, Powder Technol. 264 (2014) 536–540.
[9] S. Li, K. Kondoh, H. Imai, B. Chen, L. Jia, J. Umeda, Y. Fu, Strengthening behavior of in situ -synthesized (TiC–TiB)/ Ti composites by powder metallurgy and hot extrusion, Jmade 95 (2016) 127–132.
[10] S. LI, K. Kondoh, H. Imai, B. Chen, L. Jia, J. Umeda, Microstructure and mechanical properties of P/M titanium matrix composites reinforced by in-situ synthesized TiC–TiB, Mater. Sci. Eng. A 628 (2015) 75–83.
[11] Q. Bai, L. Zhang, L. Ke, P. Zhu, Y. Ma, S. Xia, B. Zhou, The effects of surface chemical treatment on the corrosion behavior of an Al-B4C metal matrix composite in boric acid solutions at different temperatures, Corros. Sci. 164 (2020) 108356.
[12] A. Nirala, S. Soren, N. Kumar, D.R. Kaushal, Materials today: proceedings a comprehensive review on mechanical properties of Al-B 4C stir casting fabricated composite, Mater. Today Proc. 21 (2020) 1432–1435.
[13] R.G. Lakshmikantha, V. Auradi, Materials today: proceedings processing and evaluation of Al/B4C particulate MMC ' s: tensile strength and wear properties under different elevated temperature test condition, Mater. Today Proc. 28 (2020) 504–509.
[14] D. Patidar, R.S. Rana, ScienceDirect Effect of B4C particle reinforcement on the various properties of aluminium matrix composites: a survey paper, Mater. Today Proc. 4 (2017) 2981–2988.
[15] F. Toptan, A. Rego, A.C. Alves, A. Guedes, Corrosion and tribocorrosion behavior of Ti–B4C composite intended for orthopaedic implants, J. Mech. Behav. Biomed. Mater. 61 (2016) 152–163.
[16] D. Huda, M.A. El Baradie, M.S.J. Hashmi, Metal-matrix composites: manufacturing aspects. Part I, J. Mater. Process. Technol. 37 (1993) 513–528.
[17] M.A. Awotunde, A.O. Adegbenjo, B.A. Obadele, M. Okoro, B.M. Shongwe, P.A. Olubambi, Influence of sintering methods on the mechanical properties of aluminium nanocomposites reinforced with carbonaceous compounds: a review, J. Mater. Res. Technol. 8 (2019) 2432–2449.
[18] I. Montealegre Melendez, E. Neubauer, H. Danninger, Consolidation of titanium matrix composites to maximum density by different hot pressing techniques, Mater. Sci. Eng. A 527 (2010) 4466–4473.
[19] G.I. Friedman, Titanium powder metallurgy science, Technol. Appl. (1970).
[20] H. Attar, S. Ehtemam-Haghighi, D. Kent, M.S. Dargusch, Recent developments and opportunities in additive manufacturing of titanium-based matrix composites: a review, Int. J. Mach. Tools Manuf. 133 (2018) 85–102.
[21] M. Bryant, R. Farrar, R. Freeman, K. Brummitt, J. Nolan, A. Neville, Galvanically enhanced fretting-crevice corrosion of cemented femoral stems, J. Mech. Behav. Biomed. Mater. 40 (2014) 275–286.

[22] M. Bryant, R. Farrar, R. Freeman, K. Brummitt, A. Neville, The role of surface pretreatment on the microstructure, corrosion and fretting corrosion of cemented femoral stems, Biotribology 5 (2016) 1–15.
[23] V. Singh, J.P. Shorez, N.J. Hallab, J.L. Gilbert, Material dependent fretting corrosion in spinal fusion devices: evaluation of onset and long-term response, J. Biomed. Mater. Res. 106 (2018) 2858–2868.
[24] Z. Doni, A.C. Alves, F. Toptan, J.R. Gomes, A. Ramalho, M. Buciumeanu, L. Palaghian, F.S. Silva, Dry sliding and tribocorrosion behaviour of hot pressed CoCrMo biomedical alloy as compared with the cast CoCrMo and Ti6Al4V alloys, Mater. Des. 52 (2013) 47–57.
[25] X. Zhang, W. Lu, D. Zhang, R. Wu, In situ technique for synthesizing (TiB+TiC)/Ti composites, Scr. Mater. 41 (1999) 39–46.
[26] L. Jia, S.F. Li, H. Imai, B. Chen, K. Kondoh, Size effect of B4C powders on metallurgical reaction and resulting tensile properties of Ti matrix composites by in-situ reaction from Ti-B4C system under a relatively low temperature, Mater. Sci. Eng. A 614 (2014) 129–135.
[27] Z.X. Guo, B. Derby, B. Cantor, Comparison of interfaces in Ti composites reinforced with uncoated and TiB2/C-coated SiC fibres, J. Microsc. 169 (1993) 279–287.
[28] Y.Q. Yang, H.J. Dudek, J. Kumpfert, TEM investigations of the fibre / matrix interface in SCS-6 SiC / Ti – 25Al – 10Nb – 3V – 1Mo, Interfaces (Provid.) (2000) 1235–1241.
[29] B. Choi, I.-Y. Kim, Y. Lee, Y. Kim, Microstructure and friction/wear behavior of (TiB +TiC) particulate-reinforced titanium matrix composites, Wear 318 (2014) 68–77.
[30] T. Wang, B. Gwalani, S. Shukla, M. Frank, R.S. Mishra, Development of in situ composites via reactive friction stir processing of Ti–B4C system, Compos. Part B 172 (2019) 54–60.
[31] H.T. Tsang, C.G. Chao, C.Y. Ma, Effects of volume fraction of reinforcement on tensile and creep properties of in-situ TiB/Ti MMC, Acta Metall. 37 (1997) 1359–1365.
[32] H. Attar, M. Bonisch, M. Calin, L. Zhang, S. Scudino, J. Eckert, Selective laser melting of in situ titanium–titanium boride composites: processing, microstructure and mechanical properties, Acta Mater. 76 (2014) 13–22.
[33] M.H. Loretto, D.G. Konitzer, The effect of matrix reinforcement reaction on fracture in Ti-6Ai-4V-base composites, Metall. Trans. A 21 (1990) 1579–1587.
[34] H.K.S. Rahoma, Y.Y. Chen, X.P. Wang, S.L. Xiao, Influence of (TiC+TiB) on the microstructure and tensile properties of Ti-B20 matrix alloy, J. Alloy. Compd. 627 (2015) 415–422.
[35] J. Wang, X. Guo, J. Qin, D. Zhang, W. Lu, Microstructure and mechanical properties of investment casted titanium matrix composites with B4C additions, Mater. Sci. Eng. A 628 (2015) 366–373.
[36] C. Cai, S. He, L. Li, Q. Teng, B. Song, C. Yan, Q. Wei, Y. Shi, In-situ TiB / Ti-6Al-4V composites with a tailored architecture produced by hot isostatic pressing: microstructure evolution, enhanced tensile properties and strengthening mechanisms, Compos. Part B 164 (2019) 546–558.
[37] F. Toptan, A.C. Alves, Ó. Carvalho, F. Bartolomeu, A.M.P. Pinto, F. Silva, G. Miranda, Corrosion and tribocorrosion behaviour of Ti6Al4V produced by selective laser melting and hot pressing in comparison with the commercial alloy, J. Mater. Process. Technol. 266 (2019) 239–245.
[38] E. Baril, L.P. Lefebvre, Y. Thomas, Interstitial elements in titanium powder metallurgy: sources and control, Powder Metall. 54 (2011) 183–187.
[39] A. Oliveira, F. Toptan, Wear behavior of Ti-Al2O3 biocomposites in 9 g/L NaCl solution, J. Mater. Eng. Perform. 28 (2019) 6000–6010.
[40] A. Jimoh, I. Sigalas, M. Hermann, In situ synthesis of titanium matrix composite (Ti-TiB-TiC) through sintering of TiH2 -B4C, Mater. Sci. Appl. 2012 (2012) 30–35.
[41] V.V. Patel, A. El-Desouky, J.E. Garay, K. Morsi, Pressure-less and current-activated pressure-assisted sintering of titanium dual matrix composites: effect of reinforcement particle size, Mater. Sci. Eng. A 507 (2009) 161–166, https://doi.org/10.1016/j.msea.2008.11.046
[42] B. Bobić, S. Mitrović, M. Babić, I. Bobić, Corrosion of metal-matrix composites with aluminium alloy substrate, Tribol. Ind. 32 (2010) 3–11.
[43] S.C. Ferreira, L.A. Rocha, E. Ariza, P.D. Sequeira, Y. Watanabe, J.C.S. Fernandes, Corrosion behaviour of Al/Al3Ti and Al/Al3Zr functionally graded materials produced by centrifugal solid-particle method: influence of the intermetallics volume fraction, Corros. Sci. 53 (2011) 2058–2065.
[44] Q. Feng, T. Li, H. Teng, X. Zhang, Y. Zhang, C. Liu, J. Jin, Investigation on the corrosion and oxidation resistance of Ni-Al2O3 nano-composite coatings prepared by sediment co-deposition, Surf. Coat. Technol. 202 (2008) 4137–4144.
[45] Y. Chen, J. Zhang, N. Dai, P. Qin, H. Attar, L.-C. Zhang, Corrosion behaviour of selective laser melted Ti-TiB biocomposite in simulated body fluid, Electrochim. Acta 232 (2017) 89–97.
[46] J.I. Silva, A.C. Alves, A.M. Pinto, F. Toptan, Corrosion and tribocorrosion behavior of Ti–TiB–TiNx in-situ hybrid composite synthesized by reactive hot pressing, J. Mech. Behav. Biomed. Mater. 74 (2017) 195–203.
[47] J. Bernard, S. Covino, D.E. Alman, Corrosion of Titanium Matrix Composites, Albany Res. Center, U.S. Dep. Energy, Albany, OR USA. (2002) 1–7.
[48] P. Figiel, A. Biedunkiewicz, W. Biedunkiewicz, D. Grzesiak, Evaluation of the Effect of Surface Preparation on Corrosion Properties of Cerametallic Composites in Titanium Matrix, (2016) 121–125.
[49] F. Toptan, A. Rego, A.C. Alves, A. Guedes, Corrosion and tribocorrosion behavior of Ti–B 4C composite intended for orthopaedic implants, J. Mech. Behav. Biomed. Mater. 61 (2016) 152–163.
[50] J.M. Sousa, A.C. Alves, F. Toptan, E. Ariza, A. Guedes, Corrosion and tribocorrosion behavior of Ti-B4C composites joined with TiCuNi brazing alloy, J. Mater. Eng. Perform. 28 (2019) 4972–4982, https://doi.org/10.1007/s11665-019-04217-6
[51] I. Çaha, A.C. Alves, L.J. Affonço, P.N.L. Filho, J.H.D. da Silva, L.A. Rocha, A.M.P. Pinto, F. Toptan, Corrosion and tribocorrosion behaviour of titanium nitride thin films grown on titanium under different deposition times, Surf. Coat. Technol. 374 (2019) 878–888.
[52] A. Velhinho, J.D. Botas, E. Ariza, J.R. Gomes, L.A. Rocha, Tribocorrosion Studies in Centrifugally Cast Al-matrix SiCp-reinforced Functionally Graded Composites, 456 (2004) 871–875.
[53] I. Çaha, A. Alves, C. Caterina, A. Pinto, S. Tsipas, E. Gordo, F. Toptan, Corrosion and Tribocorrosion Behavior of Ti-40Nb and Ti-25Nb-5Fe Alloys Processed by Powder Metallurgy, (n.d.).
[54] J.I. Silva, A.C. Alves, A.M. Pinto, F.S. Silva, F. Toptan, Dry sliding wear behaviour of Ti-TiB-TiN x in-situ composite synthesised by reactive hot pressing, Int. J. Surf. Sci. Eng. 10 (2016) 317–329.
[55] F. Toptan, L.A. Rocha, Tribocorrosion in metal matrix composites, in: R. Tyagi, J.P. Davim (Eds.), Processing techniques and tribological behavior of composite materials, IGI Glob., Hershey PA, 2015, pp. 149–167.